Supporting Information

Realization of isolated and high-density skyrmions at room temperature in uncompensated synthetic antiferromagnets

Ruyi Chen,[1,6] Yang Gao,[2,4,6] Xichao Zhang,[3] Ruiqi Zhang,[1] Siqi Yin,[1] Xianzhe Chen,[1] Xiaofeng Zhou,[1] Yongjian Zhou,[1] Jing Xia,[3] Yan Zhou,[3] Shouguo Wang,[4] Feng Pan,[1] Ying Zhang,[2,5*] Cheng Song[1*]

[1]Key Laboratory of Advanced Materials (MOE), School of Materials Science and Engineering, Tsinghua University, Beijing 100084, China

[2]Beijing National Laboratory for Condensed Matter Physics, Institute of Physics, Chinese Academy of Sciences, Beijing 100190, China

[3]School of Science and Engineering, The Chinese University of Hong Kong, Shenzhen, Guangdong 518172, China

[4]Institute of Advanced Materials, Beijing Normal University, Beijing 100875, China

[5]Songshan Lake Materials Laboratory, Dongguan, Guangdong 523808, China

---

[6]These authors contributed equally: R. Chen and Y. Gao.

[*]E-mail: songcheng@mail.tsinghua.edu.cn (C.S.), zhangy@iphy.ac.cn (Y.Z.)

Supplementary Note 1: Comparative experiments on the skyrmions characterization for F2 synthetic antiferromagnetic sample

To compare with the F1 sample where skyrmions can be generated via the electromagnetic coordinated method, magnetic properties and LTEM images of magnetization textures of SAF F2 are studied. Figure S1a shows the major and minor out-of-plane hysteresis loops of sample F2. The minor loop is measured by scanning perpendicular magnetic field from 500 mT to –160 mT and back to 500 mT again. Evident antiferromagnetic coupling is observed in the hysteresis loops, which favour the antiparallel alignment of the magnetization of the two ferromagnetic layers at the antiferromagnetic coupling plateau. Moreover, the positive minor-loop shift of H_{MLS} is suggestive of the AF coupling between the top and bottom Co/Pd multilayers, too. LTEM images of sample F2 at 0 mT, after applying current pulse at $\mu_0 H = 40$ mT are presented in Figure S1b. It is noted that no skyrmion is observed in F2 and it exhibits uniform state in the whole process. Figure S1c presents the anomalous Hall effect (AHE) of sample F2 measured under 0.1 mA. The anomalous Hall coefficient of our [Co/Pd] grown on an fcc Pt layer is usually different with the [Co/Pd] grown on an Ru layer due to different spin-orbit coupling and interfacial effects,[S1] leading to the discrepancy of anomalous Hall signals. The absence of the topological Hall effect signature in the transport measurement supports that there is no skyrmion in this sample.

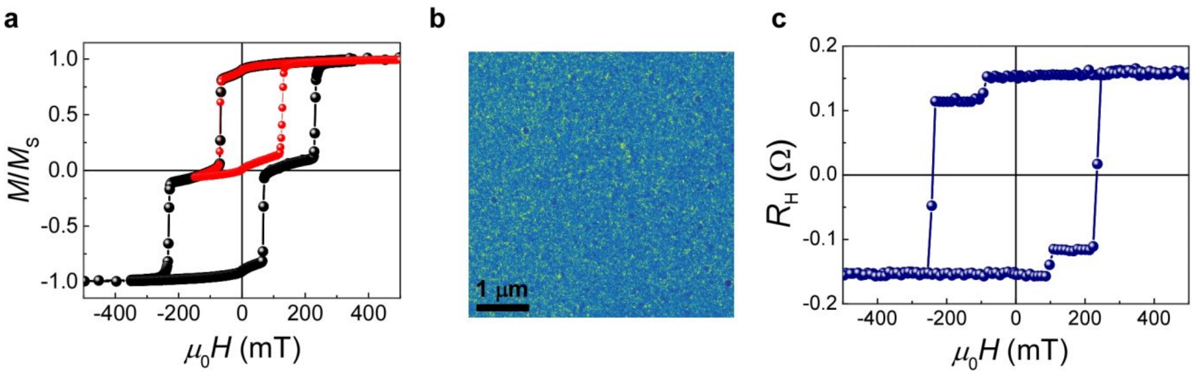

Figure S1. Magnetic properties, transport measurement and LTEM images of magnetization textures of F2 SAF. **(a)** Out-of-plane hysteresis measurement of F2 SAF. Major (black ball) and minor (red ball) hysteresis loops at room temperature are presented. **(b)** LTEM images of sample F2 at 0 mT, after applying current pulse at $\mu_0 H$ = 40 mT. **(c)** Out-of-plane AHE of sample F2 measured under 0.1 mA.

Supplementary Note 2: Experimental LTEM images of a Néel skyrmion at varying tilt angles

To further characterize the skyrmions observed in the experiment. LTEM imaging was performed at a defocus of –5 mm, at room temperature. A tilt series taken at –15°, 0° and 15° is shown in Figure S2a-c, respectively, showing the disappearance of contrast at 0° tilt and reversal of contrast for opposite tilt angles. The contrast asymmetry disappears at zero tilting angle and reverses at opposite titling angle away from zero, indicating the presence of skyrmions stable at room temperature are Néel type of skyrmions, which is a typical way to identify Néel-type skyrmion.[S2] A line profile across the structure is shown in Figure S3d. Line profiles of the three images, along the direction of the dashed line in (A), showing the differences in contrast. The skyrmion extent is determined by the distance between the maximum and minimum for the tilted samples, with a distance between maximum and minimum intensities giving a width of approximately 80 nm.

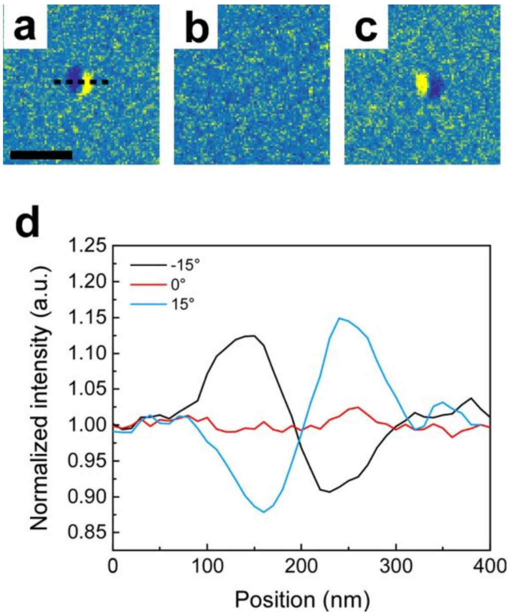

Figure S2. Experimental LTEM images of a Néel skyrmion at varying tilt angles. **(a-c)** Tilt sequence of a magnetic skyrmion with a radius of 80 nm, taken at tilting angle of (**a**) –15°, (**b**) 0° and (**c**) 15° respectively, showing the disappearance of contrast at 0° tilt and reversal of contrast for opposite tilt angles. The tilt axis is indicated by the dashed line in (**a**). Scale bar, 500 nm. (**d**) Line profiles of the three images, along the direction of the dashed line in (**a**), showing the differences in contrast. The skyrmion extent is determined by the distance between the maximum and minimum for the tilted samples.

Supplementary Note 3: Image simulation and micromagnetic modelling

The model is a ferromagnet/spacer/ferromagnet trilayer, where the top and bottom ferromagnetic layers are antiferromagnetically exchange-coupled due to the Ruderman-Kittel-Kasuya-Yosida (RKKY) mechanism. The total Hamiltonian H is decomposed into the Hamiltonian for each ferromagnetic layer H_n and the interlayer antiferromagnetic exchange coupling H_inter between neighbouring ferromagnetic layers, given as

$$H = \sum_{n=1}^{2} H_n + H_\mathrm{inter}. \tag{1}$$

The Hamiltonian for each ferromagnetic layer reads,

$$H_n = -A_{\text{intra}} \sum_{<i,j>} m_i^n \cdot m_j^n - D_{ij} \sum_{<i,j>} (\boldsymbol{v}_{ij} \times \hat{z}) \cdot (m_i^n \times m_j^n)$$

$$-K\textstyle\sum_i \left(m_i^{n,z}\right)^2 - \sum_i B \cdot m_i^n + H_{\text{DDI}}, \tag{2}$$

where n is the ferromagnetic layer index (n = 1, 2), m_i^n represents the local magnetic moment orientation normalized as $|m_i^n| = 1$ at the site i, and $<i, j>$ runs over all the nearest-neighbour sites in each ferromagnetic layer. The first term on the right-hand side of Eq. (2) represents the intralayer ferromagnetic exchange interaction with the intralayer ferromagnetic exchange constant A_{intra}. The second term represents the DMI with the DMI coupling energy D_{ij}, where $\boldsymbol{v}_{ij}$ is the unit vector between sites i and j. The third term represents the perpendicular magnetic anisotropy with the anisotropy constant K. $\boldsymbol{B}$ is the applied magnetic field. H_{DDI} represents the dipole-dipole interaction. The antiferromagnetic exchange coupling between ferromagnetic layers reads

$$H_{\text{inter}} = -A_{\text{inter}} \textstyle\sum_i m_i^1 \cdot m_i^2. \tag{3}$$

The simulation is carried out by using the Object Oriented MicroMagnetic Framework (OOMMF) software. We employed the built-in conjugate gradient (CG) minimizer for the spin relaxation simulation, which locates local minima in the energy surface through direct minimization techniques. The spin dynamics simulation is carried out by solving the Landau-Lifshitz-Gilbert (LLG) equation augmented with the damping-like spin-orbit torque.[S2] The default model is a square trilayer of 150 × 150 × 9 nm^3 with open boundary conditions. The thicknesses of the top ferromagnetic layer, spacer and bottom ferromagnetic layer are equal to 3 nm, 1 nm and 5 nm, respectively, corresponding to the sample 2 used in experiments: 2.58 nm / 0.6 nm / 5.16 nm. The cell size is set as 1 × 1 × 1 nm^3. The following magnetic parameters are used in the simulation: M_S^{bottom} = 1550 kA m^{-1}, M_S^{top} = 2150 kA m^{-1}, $A_{\text{inter}}^{\text{bottom}} = A_{\text{inter}}^{\text{top}}$ = 5~20 pJ m^{-1}, $A_{\text{intra}} = -1.0$ pJ m^{-1}, $D_{\text{bottom}} = D_{\text{top}}$ = 2.0~3.5 mJ m^{-2}, $K^{\text{bottom}} = K^{\text{top}}$ = 2.0~3.5 MJ m^{-3}. The damping parameter α = 0.1~0.3 and the spin Hall angle θ_{SH} = 0.1. Note that the values of saturation magnetization are measured by experiments, and other intrinsic magnetic parameters are adopted from Refs. [S3–S7]. Also, in all simulations we assume that the top and bottom ferromagnetic layers have the same damping parameter and gyromagnetic ratio ($\gamma = -2.211 \times 10^5$ mA^{-1}s^{-1}) for the sake of simplicity.

Supplementary Note 4: Interlayer exchange interaction dependent skyrmion phase diagram in SAF

In the left panel of Figure S3, we display the phase diagram of [Co/Pd]/Ru/[Co/Pd] SAF as a function of DMI constant D and interlayer exchange interaction constant A. Concerning the top [Co/Pd] layer of the SAF, the size of skyrmions increases with increasing D, whereas it is reduced with increasing A. Also visible is that the size of the skyrmions is reduced with increasing A for a certain D, accompanied by the absence of skyrmions with a large K and small D. A detailed inspection shows the formation of spiral states rather than skyrmions with enhancing D for a rather small A of 10 pJ m^{-1}. Similar results are obtained for the bottom [Co/Pd] layers in the right panel of Figure S3, because the top and bottom components of the skyrmions always exhibit antiferromagnetic coupling.

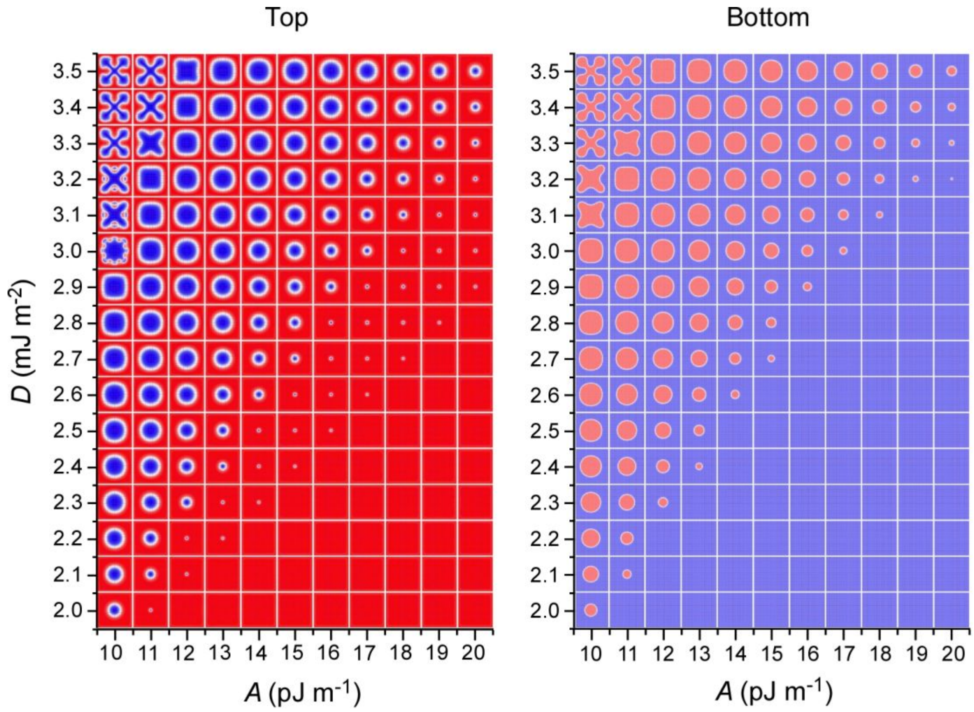

Figure S3. Simulated skyrmion phase diagram in SAF. Skyrmion phase diagram of [Co/Pd]/Ru/[Co/Pd] SAF as a function of DMI constant *D* and interlayer exchange interaction constant *A* for both top and bottom ferromagnetic layers. The out-of-plane component of spin (m_z) points along $+z$, $-z$, and in-plane are denoted by red, blue, and white, respectively.

Supplementary Note 5: Skyrmion diagram as functions of applied magnetic field and magnetic parameters in SAF

In order to get a better understanding of how the magnetic field and magnetic parameters influence the evolution of skyrmions in SAF, we have performed additional simulations on skyrmion diagram as functions of applied magnetic field B_z, DMI constant D, anisotropy constant K, and interlayer exchange interaction constant A. The simulated spin configurations and skyrmion diameter of the relaxed sample (for both top and bottom ferromagnetic layers) as functions of applied out-of-plane magnetic field B_z and DMI constant D are displayed in Fig. S4 and Fig. S5 respectively. It is noted that the skyrmions emerge and their diameters increase with the magnetic field at an appropriate value of D. Fig. S6 presents the simulated spin configurations of the relaxed sample as functions of applied out-of-plane magnetic field B_z and interlayer exchange interaction A_{inter}. It reveals that the spiral state first changes to skyrmion state and then converts to uniform magnetization state with increasing A for a certain B_z. The corresponding skyrmions size variation as functions of B_z and A is shown in Fig. S7. Besides, we display the phase diagram of SAF as a function of out-of-plane magnetic field B_z and magnetic anisotropy K in Fig. S8. Similarly, large perpendicular magnetic anisotropy favors the uniform magnetization state whereas small K leads to spiral magnetization state. Skyrmions are formed with the moderate value of K and their size change is presented in Fig. S9.

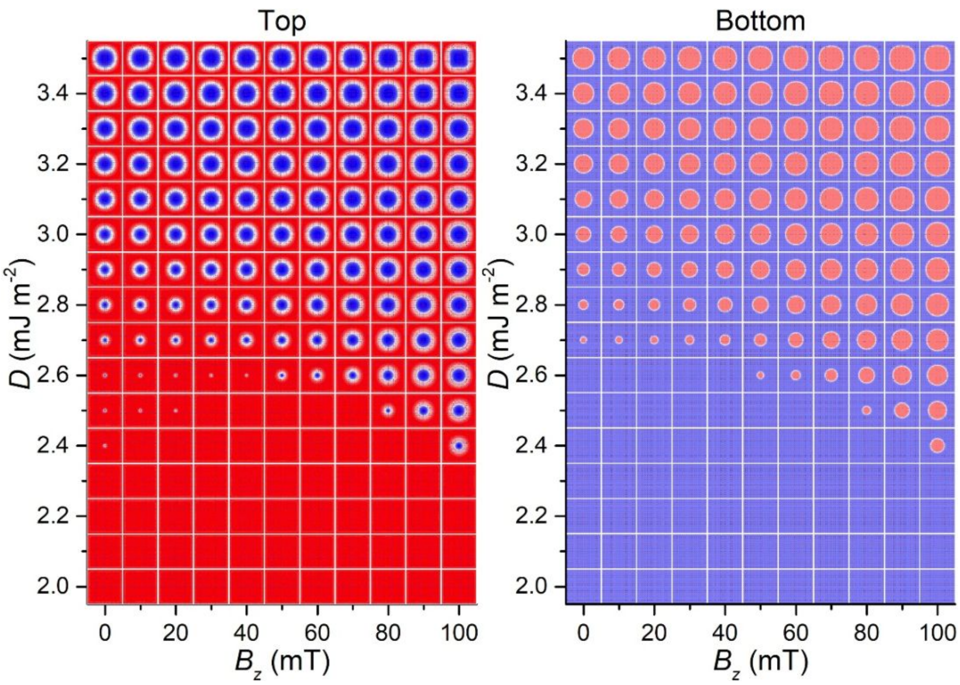

Figure S4. Simulated spin configurations (for both top and bottom ferromagnetic layers) of the relaxed sample as functions of applied out-of-plane magnetic field (B_z) and Dzyaloshinskii-Moriya interaction (D). The out-of-plane component of spin (m_z) is color coded (red is pointing along $+z$, blue is pointing along $-z$, white is in-plane).

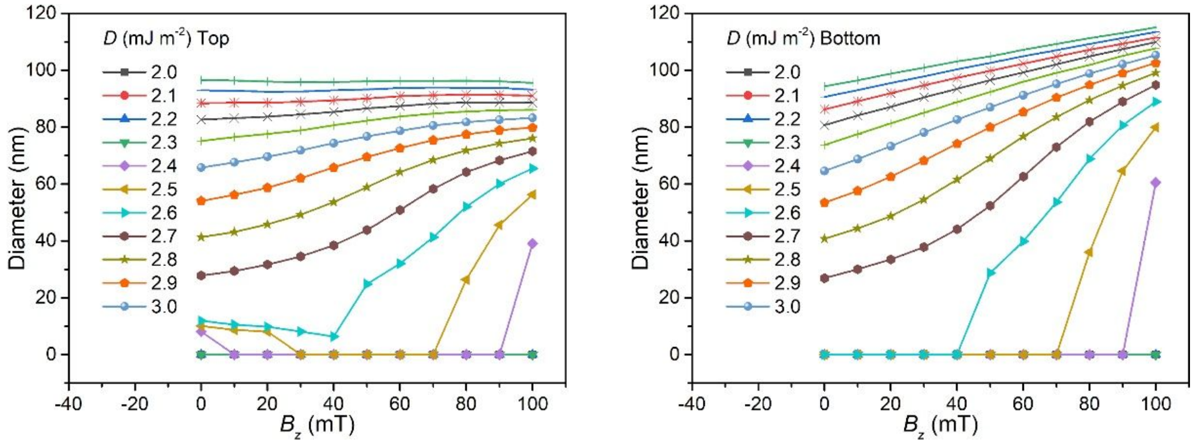

Figure S5. Relaxed skyrmion diameter as functions of applied out-of-plane magnetic field (B_z) and Dzyaloshinskii-Moriya interaction (D), corresponding to Figure S4.

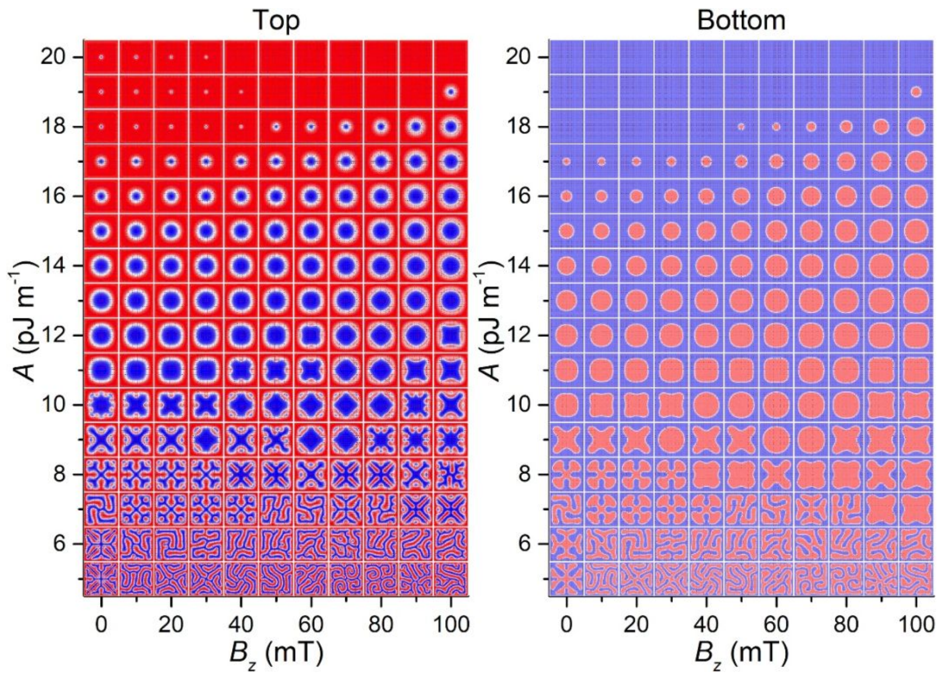

Figure S6. Simulated spin configurations (for both top and bottom ferromagnetic layers) of the relaxed sample as functions of applied out-of-plane magnetic field (B_z) and interlayer exchange interaction (A). The out-of-plane component of spin (m_z) is color coded (red is pointing along $+z$, blue is pointing along $-z$, white is in-plane).

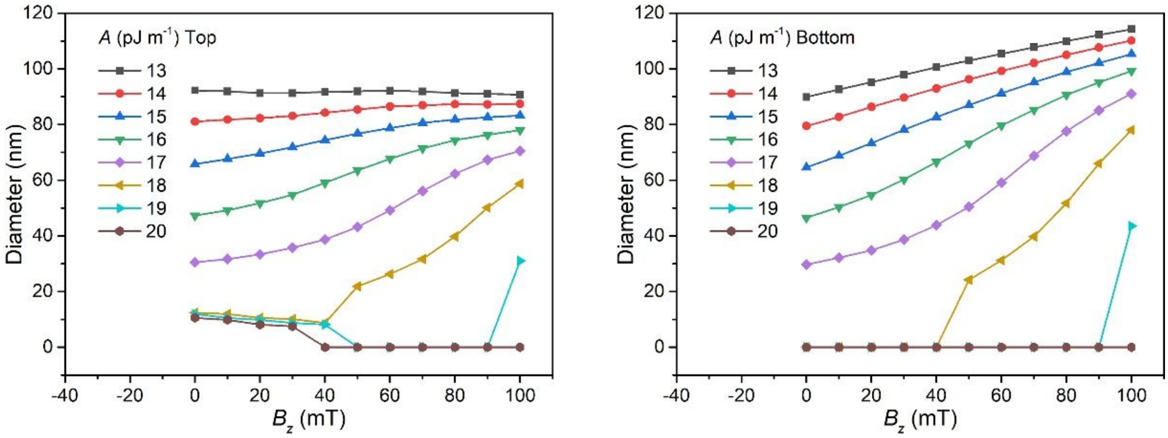

Figure S7. Relaxed skyrmion diameter as functions of applied out-of-plane magnetic field (B_z) and interlayer exchange interaction (A), corresponding to Figure S6.

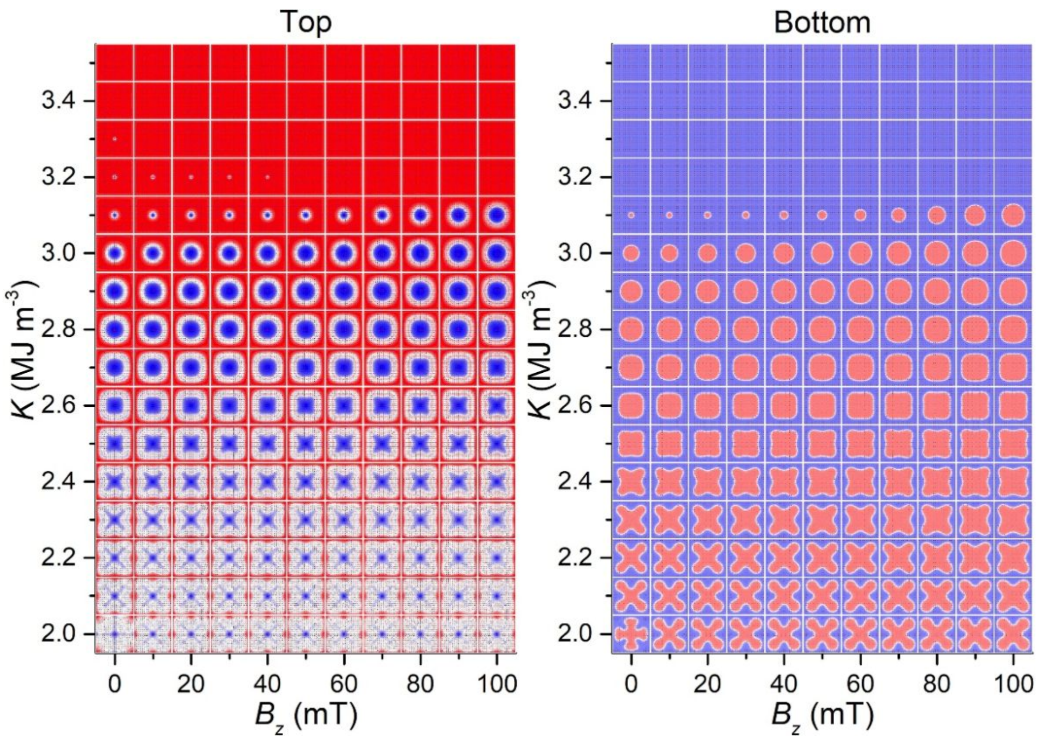

Figure S8. Simulated spin configurations (for both top and bottom ferromagnetic layers) of the relaxed sample as functions of applied out-of-plane magnetic field (B_z) and perpendicular magnetic anisotropy (K). The out-of-plane component of spin (m_z) is color coded (red is pointing along $+z$, blue is pointing along $-z$, white is in-plane).

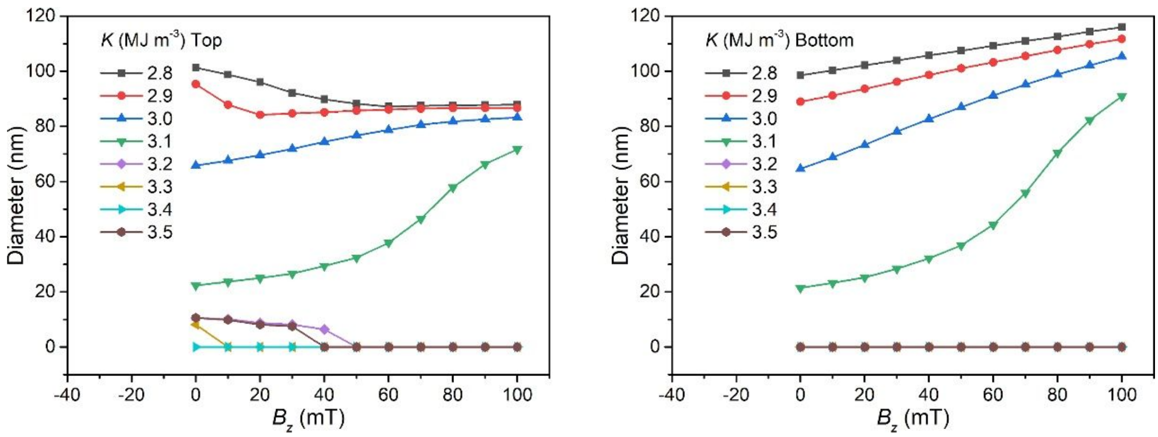

Figure S9. Relaxed skyrmion diameter as functions of applied out-of-plane magnetic field (B_z) and perpendicular magnetic anisotropy (K), corresponding to Figure S8.

Supplementary Note 6: Current-driven motion of isolated skyrmions in the synthetic antiferromagnetic bilayer with different compensation ratio

In this section, we have performed some simulations on the current-driven motion of isolated skyrmions in the synthetic antiferromagnetic bilayer with different compensation ratio. The saturation magnetization of the bottom layer is fixed at M_S^{bottom} = 2000 kA m^{-1} and the saturation magnetization of the top layer is defined as $M_S^{\mathrm{top}} = nM_S^{\mathrm{bottom}}$, where n being the compensation ratio. n ranges between 0.9 and 1.02 where skyrmion is metastable state in the bilayer. The driving current density j = 50 MA cm^{-2} and the spin Hall angle θ_{SH} = 0.1. The spin current is injected into both top and bottom layers with polarization directions pointing along $\pm y$ directions. The velocity of skyrmion motion in SAF increases with n changes from 0.90 to 1.02 as displayed in Fig. S10a. It is worth noting that the skyrmion Hall angle θ_{SkHE} vanishes when n becomes 1.00 corresponding the compensated SAF. The skyrmion moves straightly in the compensated scenario (n = 1.00) and obvious lateral shift are observed in the uncompensated structures (n = 0.90, n = 1.02). Corresponding movies showing the skyrmion motion at selected compensation ratio n and damping constant α are provided as supplementary files. For a given damping constant α, the diameter of the skyrmion increases from 10 nm to 50 nm as n increases from 0.90 to 1.02.

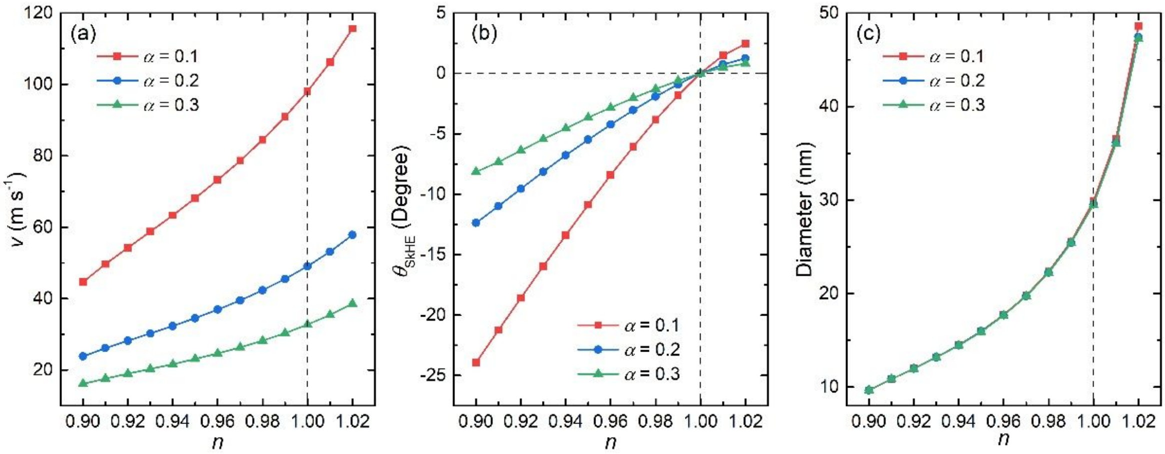

Figure S10. Current-driven motion of skyrmion in the antiferromagnetically exchange-coupled bilayer. (a) Skyrmion velocity as functions of compensation ratio n and damping constant α. (b) Skyrmion Hall angle θ_{SkHE} as functions of compensation ratio n and damping constant α. (c) Skyrmion diameter as functions of compensation ratio n and damping constant α. Note that the simulated model is a square trilayer of 150 × 150 × 9 nm^3 with periodic boundary conditions. The thicknesses of the top ferromagnetic layer, spacer and bottom ferromagnetic layer are equal to 3 nm, 1 nm and 5 nm. Here, $A_{\mathrm{inter}}^{\mathrm{bottom}} = A_{\mathrm{inter}}^{\mathrm{top}} = 15$ pJ m^{-1}, $A_{\mathrm{intra}} = -1.0$ pJ m^{-1}, $D_{\mathrm{bottom}} = D_{\mathrm{top}} = 3.0$ mJ m^{-2}, $K^{\mathrm{bottom}} = K^{\mathrm{top}} = 3.0$ MJ m^{-3}.

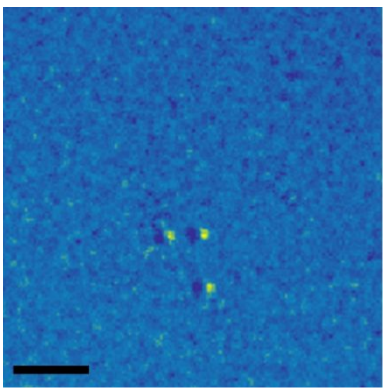

Figure S11. Under-focused LTEM images of [Co/Pd]/Ru/[Co/Pd]/Ru/[Co/Pd] SAF with three ferromagnetic layers recorded at 18 mT after being saturated. The scale bar in LTEM images corresponds to 1 μm.

Supplementary Movie 1:

This movie shows the motion of isolated skyrmion induced by current in SAF at the compensation ratio n = 0.90 and damping constant α = 0.3.

Supplementary Movie 2:

This movie shows the motion of isolated skyrmion induced by current in SAF at the compensation ratio n = 1.00 and damping constant α = 0.3.

Supplementary Movie 3:

This movie shows the motion of isolated skyrmion induced by current in SAF at the compensation ratio n = 1.02 and damping constant α = 0.3.

Supplementary references:

[S1.] Zhang, P. X.; Liao, L. Y.; Shi, G. Y.; Zhang, R. Q.; Wu, H. Q.; Wang, Y. Y.; Pan, F.; Song, C. *Phys. Rev. B* **2018**, 97, 214403.

[S2.] Pollard, S. D.; Garlow, J. A.; Yu, J.; Wang, Z.; Zhu, Y.; Yang, H. Observation of stable Néel skyrmions in cobalt/palladium multilayers with Lorentz transmission electron microscopy. *Nat. Commun.* **2017**, 8, 14761.

[S3.] Zhang, X.; Ezawa, M.; Zhou, Y. Thermally stable magnetic skyrmions in multilayer synthetic antiferromagnetic racetracks. *Phys. Rev. B* **2016**, 94, 064406.

[S4.] Tomasello R.; Martinez E.; Zivieri R.; Torres L.; Carpentieri M.; Finocchio G. A strategy for the design of skyrmion racetrack memories. *Sci. Rep.* **2014**, 4, 6784.

[S5] Zhang, X.; Zhou, Y.; Ezawa, M. Magnetic bilayer-skyrmions without skyrmion Hall effect. *Nat. Commun.* **2016**, 7, 10293.

[S6] Sampaio, J.; Cros, V.; Rohart, S.; Thiaville, A.; Fert, A. Nucleation, stability and current-induced motion of isolated magnetic skyrmions in nanostructures. *Nat. Nanotechnol.* **2013**, 8, 839.

[S7] Zhang J.; Ho P.; Currivan-Incorvia J.; Siddiqui S.; Baldo M.; Ross C. Edge-modulated perpendicular magnetic anisotropy in [Co/Pd]n and L10-FePt thin film wires. *Appl. Phys. Lett*. **2015**, 107, 182408.